Abstract #02844 ISMRM ABSTRACT

Validity of the Gaussian phase approximation (GPA): Analytical results for the constant gradient spin echo in one dimension

Primary: Diffusion - Diffusion Modeling 〉 **Secondary:** Diffusion - Simulation/Validation 〉 **Presentation:** Oral, PowerPitch Oral, Digital Poster 〉 **Keywords:** DIFFUSION MODELING NON-GAUSSIAN DIFFUSION TEMPORAL DIFFUSION SPECTROSCOPY DIFFUSION MICROSTRUCTURE PHASE KURTOSIS

Teddy X Cai [1], **Nathan H Williamson**[1,2,3], **Peter J Basser**[1]

[1]Section on Quantitative Imaging and Tissue Sciences (SQITS), Eunice Kennedy Shriver - National Institute of Child Health and Human Development (NICHD), Bethesda, United States of America
[2]The Henry M. Jackson Foundation for the Advancement of Military Medicine, Inc., Bethesda, United States of America
[3]Uniformed Services University of the Health Sciences, Bethesda, United States of America

Presenting Author: *Teddy X Cai (teddy.cai@nih.gov)*

Impact

We find that the GPA is more fragile than commonly assumed. The introduction of exchange-like dynamics, in particular, can lead to significant positive excess phase kurtosis. This undermines the validity of models that assume the GPA in permeable microstructure.

Synopsis

Motivation:	The GPA underlies many diffusion signal models, such as temporal diffusion spectroscopy (TDS), yet its validity is rarely scrutinized.
Goals:	To interrogate the GPA by analytically deriving the excess phase kurtosis, which directly quantifies non-Gaussianity in the phase distribution.
Approach:	Three paradigmatic, one-dimensional systems were studied: (1) Poisson pore-hopping, (2) trapping-release with an exponentially-distributed release time, and (3) restriction. The excess phase kurtosis was derived for the constant gradient spin echo.
Results:	Pore-hopping and trapping-release dynamics yield positive excess kurtosis for few hops and slow release, respectively. Restriction yields complicated behavior, with both negative (short-time) and positive (longer-time) kurtotic regimes.

Introduction

The GPA[1-3] posits that the spin phase distribution $P(\phi)$ has negligible higher-order cumulants. It is implied in models based on second-order motion statistics, e.g., diffusion tensor imaging (DTI).[4] It is explicitly invoked in TDS[5-8] and to describe motional averaging.[2,9] While widely assumed, the GPA is rarely scrutinized, despite known cases of breakdown, such as the localization regime.[10-12] Various simulation studies also report significant deviations from the GPA for restriction.[13-16]

Understanding when the GPA is valid is essential for accurate modeling. A direct diagnostic is the excess phase kurtosis, κ_4/κ_2^2, where κ_n denotes the n^{th} phase cumulant. Though kurtosis has been studied in the diffusional kurtosis model,[17,18] these works were based on displacement kurtosis. Phase and displacement are not generally bijective — this holds only for (infinitesimally) narrow gradients. With finite gradients, trajectory determines phase.

We derive analytical forms of κ_4/κ_2^2 in paradigmatic, one-dimensional systems: (1) Poisson pore-hopping, (2) trapping-release with an exponentially-distributed release time, and (3) restriction. The spin echo with constant gradient amplitude[19] is considered. To our knowledge, these represent the first analytical results for κ_4/κ_2^2 in non-trivial systems without assuming Gaussian compartments[20] and/or narrow gradients.

Basic theory

The relaxation-normalized echo signal S can be expanded as[5,6,20]

$$\ln S = \sum_{n=1}^{\infty} \frac{\mathrm{i}^n}{n!}\kappa_n.$$

For symmetric motion, which we assume throughout, odd cumulants vanish. The GPA corresponds to a second-order approximation, denoted

$$\ln S^{(2)} = -\frac{\kappa_2}{2} \propto -g^2,$$

where $\kappa_2 = \langle\phi^2\rangle$, $\langle\cdot\rangle$ denotes ensemble averaging, and g is gradient amplitude. To fourth-order:

$$\ln S^{(4)} = -\frac{\kappa_2}{2} + \frac{\kappa_4}{24},$$

where $\kappa_4 = \langle\phi^4\rangle - 3\langle\phi^2\rangle^2$. The excess phase kurtosis is

$$\mathrm{Kurt}(\phi) - 3 = \frac{\langle\phi^4\rangle}{\langle\phi^2\rangle^2} - 3 = \frac{\kappa_4}{\kappa_2^2}.$$

Finding κ_4/κ_2^2 reduces to finding phase moments. The n^{th} moment is given by an n-fold time integral over the n-point displacement correlator and $G(t)$, where $G(t)$ is the gradient waveform scaled by (proton) gyromagnetic ratio $\gamma \approx 2.675 \times 10^8\ \text{T}^{-1}\text{s}^{-1}$. Here, $G(t) = \gamma g$ for $0 \leq t \leq T/2$ and $-\gamma g$ for $T/2 < t \leq T$, where T denotes echo time; $T = 10\ \text{ms}$ throughout. Explicitly,

$$\langle \phi^4 \rangle = \int_0^T \int_0^T \int_0^T \int_0^T G(t_1)G(t_2)G(t_3)G(t_4)C(t_1,t_2,t_3,t_4)dt_1dt_2dt_3dt_4,$$

where

$$C(t_1,t_2,t_3,t_4) = \langle r(t_1)r(t_2)r(t_3)r(t_4)\rangle,$$

and

$$r(t) = x(t) - x(0)$$

is the displacement trajectory. Below, the analytical κ_4/κ_2^2 is derived for each system. For brevity, only system specifications and final results are given.

Model 1: Poisson pore-hopping

Assume $r(t)$ obeys the Poisson process:

$$r(t) = \Delta x \sum_{j=1}^{H(t)} \zeta_j,$$

where Δx is a uniform pore spacing, ζ_j are random variables taking ± 1 with equal probability, and $H(t)$ is the hop count with probability

$$P(H(t) = h) = \frac{(t/\tau_{\text{hop}})^h}{h!} e^{-t/\tau_{\text{hop}}},$$

where τ_{hop} is the mean inter-hop time. This is a simplified representation of small, periodic pores separated by weakly permeable barriers. The signal is exactly

$$\ln S = \frac{2}{\tau_{\text{hop}}} \left[\frac{\sin(\gamma g \Delta x (T/2))}{\gamma g \Delta x} - \frac{T}{2} \right],$$

and the even cumulants are

$$\kappa_n = \frac{1}{\tau_{\text{hop}}} \frac{(\gamma g \Delta x)^n\, T^{n+1}}{2^n (n+1)}.$$

Thus,

$$\frac{\kappa_4}{\kappa_2^2} = \frac{9}{5} \frac{\tau_{\text{hop}}}{T}.$$

See Figure 1 for signal behavior.

Model 2: Trapping-release with exponentially-distributed release time

Assume spins are initially immobilized and released with diffusivity D at release time τ_{rel}, drawn from

$$P(\tau_{\text{rel}}) = k e^{-k\tau_{\text{rel}}},$$

where $k = 1/\langle \tau_{\text{rel}} \rangle$, and $\langle \tau_{\text{rel}} \rangle$ is the mean release time. This is a simplified representation of barrier-limited exchange with a free compartment. One finds

$$\langle \phi^2 \rangle = \gamma^2 g^2 T^3 D \left(\frac{1}{6} - \frac{4}{\alpha^3} \left[1 - e^{-\alpha} - \alpha e^{-\alpha/2} \right] \right),$$

and

$$\langle \phi^4 \rangle = \frac{\gamma^4 g^4 D^2 T^6}{12\alpha^6} \left(\alpha^6 + 24\alpha^4 e^{-\alpha/2} - \alpha^3 \left[48 + 432\, e^{-\alpha/2} \right] + 11,520 \left[1 - e^{-\alpha} - \alpha e^{-\alpha/2} \right] \right),$$

where $\alpha = kT$. See Figure 2 for κ_4/κ_2^2 and Figure 3 for signal behavior. Monte Carlo simulated data are also presented.

Model 3: Restricted diffusion

Consider restricted diffusion in domain size L with well-known propagator

$$P(x, t \mid x_0) = \frac{1}{L} + \sum_{m=1}^{\infty} \psi_m(x) \psi_m(x_0) e^{-\lambda_m t},$$

where

$$\psi_m(x) = \sqrt{\frac{2}{L}} \cos\left(\frac{m\pi x}{L}\right), \quad \lambda_m = D\left(\frac{m\pi}{L}\right)^2.$$

It is known[2] that

$$\langle \phi^2 \rangle = \frac{16\gamma^2 g^2 L^4}{D\pi^6} \sum_{m \geq 1,\ \text{odd}}^{\infty} \frac{T - \lambda_m^{-1}\left(3 - 4e^{-\lambda_m T/2} + e^{-\lambda_m T}\right)}{m^6}.$$

One finds

$$\langle \phi^4 \rangle = \frac{32 L^4}{\pi^8} \sum_{a \geq 1,\ \text{odd}}^{\infty} \sum_{c \geq 1,\ \text{odd}}^{\infty} \left(\frac{2 I_{a,c}}{a^4 c^4} + \sum_{b \geq 2,\ \text{even}}^{\infty} \frac{I_{a,b,c}}{a^2 c^2} \left[\frac{1}{(a-b)^2} + \frac{1}{(a+b)^2} \right] \left[\frac{1}{(b-c)^2} + \frac{1}{(b+c)^2} \right] \right),$$

where $I_{a,c}$ and $I_{a,b,c}$ denote tedious but piecewise solvable integrals:

$$I_{a,c} = \sum_{\text{perms } t_1,t_2,t_3,t_4} \int_0^T \int_0^T \int_0^T \int_0^T G(t_1) G(t_2) G(t_3) G(t_4) e^{-\lambda_a (t_2' - t_1')} e^{-\lambda_c (t_4' - t_3')} dt_1' dt_2' dt_3' dt_4',$$

and

$$I_{a,b,c} = \sum_{\text{perms } t_1,t_2,t_3,t_4} \int_0^T \int_0^T \int_0^T \int_0^T G(t_1) G(t_2) G(t_3) G(t_4) e^{-\lambda_a (t_2' - t_1')} e^{-\lambda_b (t_3' - t_2')} e^{-\lambda_c (t_4' - t_3')} dt_1' dt_2' dt_3' dt_4',$$

where this sum denotes permutations of $\{t_1, t_2, t_3, t_4\}$ mapped to the ordered set of integration variables: $t_1' \leq t_2' \leq t_3' \leq t_4'$. For example, $\{t_1', t_2', t_3', t_4'\} \rightarrow \{t_4, t_3, t_2, t_1\}$ implies $t_4 \leq t_3 \leq t_2 \leq t_1$. See Figure 4 for κ_4/κ_2^2 and Figure 5 for signal behavior. Figure data was truncated at $a, b, c, m \leq 101$.

Discussion/Conclusion

Results indicate the GPA is fragile, at least for this experiment. Considering the heuristic $\kappa_4/\kappa_2^2 \lesssim 0.1$, the GPA holds for $T/\tau_{\text{hop}} \gtrsim 18$, $\alpha \gtrsim 6$, and $L/\sqrt{DT} \gtrsim 20$ in each model, respectively, though the latter exhibits complicated intermediate behavior. Overall, κ_4/κ_2^2 is usually positive, and can become large for exchange-like behavior, as in Models 1 and 2.

This study, though limited to one-dimensional systems and one experiment, has wide-ranging implications. Importantly, it suggests that in permeable microstructure, the GPA may be violated. This is consequential, e.g., for DTI[21,22] and TDS[23,24] works in gray matter, which is known to abundantly express water channels.[25] Additionally, these results challenge the notion of motional averaging,[2,9] as small $L/\sqrt{DT} \approx 0.1 - 2$ does not have near-zero κ_4/κ_2^2 via a central limit theorem argument, but rather negative κ_4/κ_2^2. Consider that numerous multi-compartment signal models (e.g., CHARMED,[26] SANDI[27]) make use of a motional averaging approximation.[3]

To conclude, novel analytical results for the excess phase kurtosis were derived, with cautionary implications.

Acknowledgements

This research was supported by the Intramural Research Program of the Eunice Kennedy Shriver National Institute of Child Health and Human Development (NICHD). This research was supported in part by the Intramural Research Program of the National Institutes of Health (NIH). This work was partially funded by the Department of Defense in the Military Traumatic Brain Injury Initiative (MTBI^2) under award HU0001-24-2-0051.

References

1. Carr HY, Purcell EM. Effects of Diffusion on Free Precession in Nuclear Magnetic Resonance Experiments. Physical Review. 1954;94(3):630-8. doi: 10.1103/physrev.94.630

2. Neuman CH. Spin echo of spins diffusing in a bounded medium. The Journal of Chemical Physics. 1974;60(11):4508-11. doi: 10.1063/1.1680931

3. Novikov DS, Fieremans E, Jespersen SN, Kiselev VG. Quantifying brain microstructure with diffusion MRI: Theory and parameter estimation. NMR in Biomedicine. 2019;32(4). doi: 10.1002/nbm.3998

4. Basser P, Mattiello J, LeBihan D. MR diffusion tensor spectroscopy and imaging. Biophysical Journal. 1994;66(1):259-67. doi: 10.1016/S0006-3495(94)80775-1

5. Stepišnik J. Analysis of NMR self-diffusion measurements by a density matrix calculation. Physica B+C. 1981;104(3):350-64. doi: 10.1016/0378-4363(81)90182-0

6. Stepišnik J. Time-dependent self-diffusion by NMR spin-echo. Physica B: Condensed Matter. 1993;183(4):343-50. doi: 10.1016/0921-4526(93)90124-o

7. Callaghan PT, Stepišnik J. Frequency-Domain Analysis of Spin Motion Using Modulated-Gradient NMR. Journal of Magnetic Resonance, Series A. 1995;117(1):118-22. doi: 10.1006/jmra.1995.9959

8. Parsons EC, Does MD, Gore JC. Temporal diffusion spectroscopy: Theory and implementation in restricted systems using oscillating gradients. Magnetic Resonance in Medicine. 2006;55(1):75-84. doi: 10.1002/mrm.20732

9. Hürlimann M, Helmer K, Deswiet T, Sen P. Spin Echoes in a Constant Gradient and in the Presence of Simple Restriction. Journal of Magnetic Resonance, Series A. 1995;113(2):260-4. doi: 10.1006/jmra.1995.1091

10. Stoller SD, Happer W, Dyson FJ. Transverse spin relaxation in inhomogeneous magnetic fields. Physical Review A. 1991;44(11):7459-77. doi: 10.1103/physreva.44.7459

11. de Swiet TM, Sen PN. Time dependent diffusion coefficient in a disordered medium. The Journal of Chemical Physics. 1996;104(1):206-9. doi: 10.1063/1.470890

12. Moutal N, Grebenkov DS. The localization regime in a nutshell. Journal of Magnetic Resonance. 2020;320:106836. doi: 10.1016/j.jmr.2020.106836

13. Balinov B, Jonsson B, Linse P, Soderman O. The NMR Self-Diffusion Method Applied to Restricted Diffusion. Simulation of Echo Attenuation from Molecules in Spheres and between Planes. Journal of Magnetic Resonance, Series A. 1993;104(1):17-25. doi: 10.1006/jmra.1993.1184

14. Blees M. The Effect of Finite Duration of Gradient Pulses on the Pulsed-Field-Gradient NMR Method for Studying Restricted Diffusion. Journal of Magnetic Resonance, Series A. 1994;109(2):203-9. doi: 10.1006/jmra.1994.1156

15. Sukstanskii AL, Yablonskiy DA. Effects of Restricted Diffusion on MR Signal Formation. Journal of Magnetic Resonance. 2002;157(1):92-105. doi: 10.1006/jmre.2002.2582

16. Topgaard D. Validity of the Gaussian phase distribution approximation for analysis of isotropic diffusion encoding applied to restricted diffusion in a cylinder. Magnetic Resonance Letters. 2025. In Press. doi: 10.1016/j.mrl.2025.200196

17. Jensen JH, Helpern JA, Ramani A, Lu H, Kaczynski K. Diffusional kurtosis imaging: The quantification of non-gaussian water diffusion by means of magnetic resonance imaging. Magnetic Resonance in Medicine. 2005;53(6):1432-40. doi: 10.1002/mrm.20508

18. Jensen JH, Helpern JA. MRI quantification of non-Gaussian water diffusion by kurtosis analysis. NMR in Biomedicine. 2010;23(7):698-710. doi: 10.1002/nbm.1518

19. Hahn EL. Spin Echoes. Physical Review. 1950;80(4):580-94. doi: 10.1103/physrev.80.580

20. Ning L, Nilsson M, Lasič S, Westin C, Rathi Y. Cumulant expansions for measuring water exchange using diffusion MRI. The Journal of Chemical Physics. 2018;148(7):074109. doi: 10.1063/1.5014044

21. Mukherjee P, Miller JH, Shimony JS, et al. Diffusion-tensor MR imaging of gray and white matter development during normal human brain maturation. AJNR Am J Neuroradiol. 2002;23(9):1445-56. PMID: 12372731 [pmid]

22. Pfefferbaum A, Adalsteinsson E, Rohlfing T, Sullivan EV. Diffusion tensor imaging of deep gray matter brain structures: Effects of age and iron concentration. Neurobiology of Aging. 2010;31(3):482-93. doi: 10.1016/j.neurobiolaging.2008.04.013

23. Dai E, Zhu A, Yang GK, et al. Frequency-dependent diffusion kurtosis imaging in the human brain using an oscillating gradient spin echo sequence and a high-performance head-only gradient. NeuroImage. 2023;279:120328. doi: 10.1016/j.neuroimage.2023.120328

24. Yon M, Narvaez O, Topgaard D, Sierra A. In vivo rat brain mapping of multiple gray matter water populations using nonparametric D(ω)-R1-R2 distributions MRI. NMR in Biomedicine. 2025;38(1):Epub. doi: 10.1002/nbm.5286

25. Mader S, Brimberg L. Aquaporin-4 Water Channel in the Brain and Its Implication for Health and Disease. Cells. 2019;8(2):90. doi: 10.3390/cells8020090

26. Assaf Y, Basser PJ. Composite hindered and restricted model of diffusion (CHARMED) MR imaging of the human brain. NeuroImage. 2005;27(1):48-58. doi: 10.1016/j.neuroimage.2005.03.042

27. Palombo M, Ianus A, Guerreri M, et al. SANDI: A compartment-based model for non-invasive apparent soma and neurite imaging by diffusion MRI. NeuroImage. 2020;215:116835. doi: https://doi.org/10.1016/j.neuroimage.2020.116835

Figures and Tables

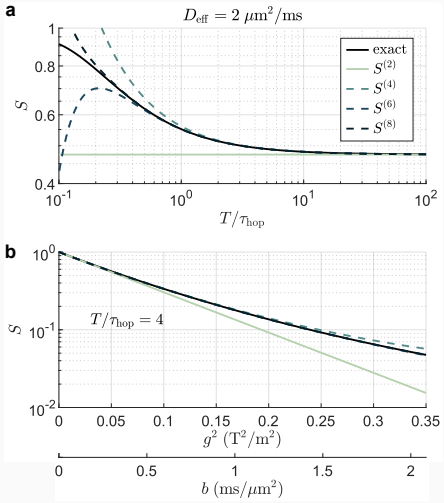

Figure 1: *Signal for the Poisson pore-hopping model. (a) Signal vs. T/τ_{hop}. The exact signal (black) is compared to the GPA (light-green) and higher-order approximations (dashed). The effective diffusivity $D_{\mathrm{eff}}=(\Delta x)^2/2\tau_{\mathrm{hop}}$ and $T=10\;\mathrm{ms}$ were fixed. (b) Signal vs. $g^2\propto b$-value $=\gamma^2g^2T^3/12$ for fixed hop number (same legend). The GPA decays linearly.*

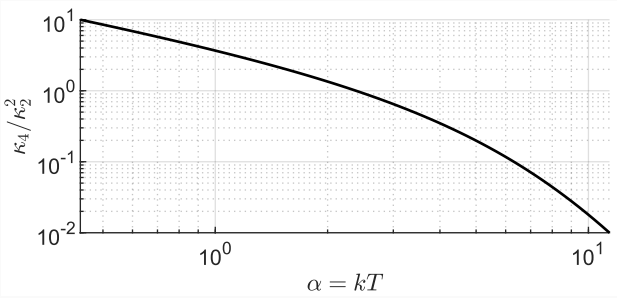

Figure 2: *Excess phase kurtosis in the trapping-release model vs. $\alpha = kT$, with $T=10\;\mathrm{ms}$ and $D=2\;\mathrm{\mu m^2/ms}$. The released spin fraction is given by $1-e^{-\alpha}$. Note the roughly log-linear decay at small α, accelerating as $\alpha\gtrsim 5$. The GPA can be said to hold for $\alpha\gtrsim 6$ using the heuristic $\kappa_4/\kappa_2^2\lesssim 0.1$.*

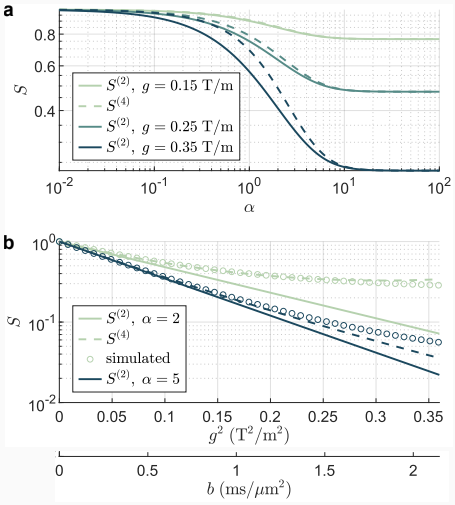

Figure 3: *Signal for the trapping-release model with the same parameters as Figure 2. (a) Signal vs. α for various g (colors). Second- (solid) and fourth-order (dashed) approximations are shown. (b) Signal vs. g^2 or b for fixed values of α (colors). Data from Monte Carlo simulations (circles) are also shown. Note the sub-linear decay of simulated data and higher-order approximations, consistent with positive excess phase kurtosis.*

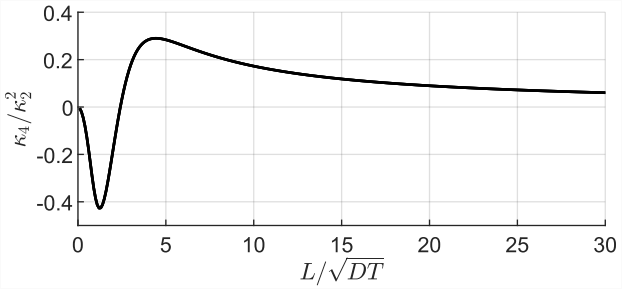

Figure 4: *Excess phase kurtosis for restriction vs. $L/\sqrt{DT}$, with $T=10\;\mathrm{ms}$ and $D=2\;\mathrm{\mu m^2/ms}$. Data were generated by truncating the eigensum at integer index 101. Note the negative and positive peaks at $L/\sqrt{DT}\approx 1.8$ and $L/\sqrt{DT}\approx4.4$, respectively. The negative regime arises from truncated tails, while the positive regime arises from a central peak in $P(\phi)$ due to reflections.*

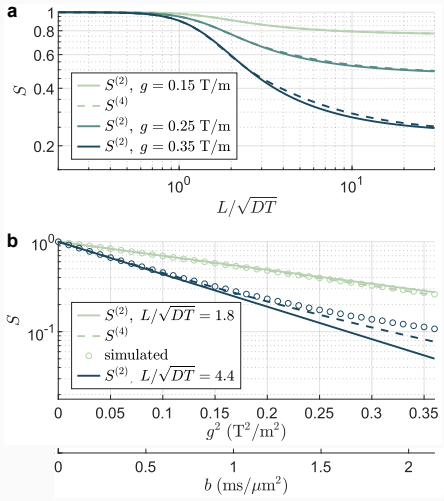

Figure 5: *Signal for restriction with the same parameters as Figure 4. (a) Signal vs. $L/\sqrt{DT}$ for various g. Second- (solid) and fourth-order (dashed) approximations are shown. (b) Signal vs. g^2 or b for fixed values of $L/\sqrt{DT}$ (colors). Data from Monte Carlo simulations (circles) are also shown. Note for $L/\sqrt{DT}=1.8$, corresponding to the negative regime in Figure 4, there is slight super-linear decay, consistent with negative excess phase kurtosis.*